



**HAL**  
open science

## Complex lithospheric structure under the central Baltic Shield from surface wave tomography.

M. Bruneton, Helle A. Pedersen, Véronique Farra, Nicholas Arndt, P. Vacher, U. Achauer, A. Alinaghi, J. Ansorge, G. Bock, W. Friederich, et al.

► **To cite this version:**

M. Bruneton, Helle A. Pedersen, Véronique Farra, Nicholas Arndt, P. Vacher, et al.. Complex lithospheric structure under the central Baltic Shield from surface wave tomography.. *Journal of Geophysical Research: Solid Earth*, 2004, 109 (B10) (B10), pp.B10303. 10.1029/2003JB002947 . hal-00109927

**HAL Id: hal-00109927**

**<https://hal.science/hal-00109927>**

Submitted on 30 Jul 2020

**HAL** is a multi-disciplinary open access archive for the deposit and dissemination of scientific research documents, whether they are published or not. The documents may come from teaching and research institutions in France or abroad, or from public or private research centers.

L'archive ouverte pluridisciplinaire **HAL**, est destinée au dépôt et à la diffusion de documents scientifiques de niveau recherche, publiés ou non, émanant des établissements d'enseignement et de recherche français ou étrangers, des laboratoires publics ou privés.

## Complex lithospheric structure under the central Baltic Shield from surface wave tomography

Marianne Bruneton,<sup>1</sup> Helle A. Pedersen,<sup>1,2</sup> Véronique Farra,<sup>3</sup> Nicholas T. Arndt,<sup>4</sup> Pierre Vacher,<sup>5</sup> U. Achauer,<sup>6</sup> A. Alinaghi,<sup>7</sup> J. Ansorge,<sup>8</sup> G. Bock,<sup>7,9</sup> W. Friederich,<sup>10</sup> M. Grad,<sup>11</sup> A. Guterch,<sup>12</sup> P. Heikkinen,<sup>13</sup> S.-E. Hjelt,<sup>14</sup> T. L. Hyvönen,<sup>13</sup> J.-P. Ikonen,<sup>13</sup> E. Kissling,<sup>8</sup> K. Komminaho,<sup>14</sup> A. Korja,<sup>13</sup> E. Kozlovskaya,<sup>14</sup> M. V. Nevsky,<sup>15</sup> H. Paulssen,<sup>16</sup> N. I. Pavlenkova,<sup>15</sup> J. Plomerová,<sup>17</sup> T. Raita,<sup>14</sup> O. Y. Riznichenko,<sup>15</sup> R. G. Roberts,<sup>18</sup> S. Sandoval,<sup>8</sup> I. A. Sanina,<sup>15</sup> N. V. Sharov,<sup>19</sup> Z. H. Shomali,<sup>18</sup> J. Tiikkainen,<sup>14</sup> E. Wielandt,<sup>10</sup> K. Willegalla,<sup>7</sup> J. Yliniemi,<sup>20</sup> and Y. G. Yurov<sup>21</sup>

Received 19 December 2003; revised 17 May 2004; accepted 9 June 2004; published 8 October 2004.

[1] Regional seismic tomography provides valuable information on the structure of shields, thereby gaining insight to the formation and stabilization of old continents. Fennoscandia (known as the Baltic Shield for its exposed part) is a composite shield for which the last recorded tectonic event is the intrusion of the Rapakivi granitoids around 1.6 Ga. A seismic experiment carried out as part of the European project Svecofennian-Karelia-Lapland-Kola (SVEKALAPKO) was designed to study the upper mantle of the Finnish part of the Baltic Shield, especially the boundary between Archean and Proterozoic domains. We invert the fundamental mode Rayleigh waves to obtain a three-dimensional shear wave velocity model using a ray-based method accounting for the curvature of wave fronts. The experiment geometry allows an evaluation of lateral variations in velocities down to 150 km depth. The obtained model exhibits variations of up to  $\pm 3\%$  in  $S$  wave velocities. As the thermal variations beneath Finland are very small, these lateral variations must be caused by different rock compositions. The lithospheres beneath the Archean and Proterozoic domains are not noticeably different in the  $S$  wave velocity maps. A classification of the velocity profiles with depth yields four main families and five intermediate regions that can be correlated with surface features. The comparison of these profiles with composition-based shear wave velocities implies both lateral and vertical variations of the mineralogy. *INDEX TERMS:* 7218 Seismology: Lithosphere and upper mantle; 7255 Seismology: Surface waves and free oscillations; 8180 Tectonophysics: Tomography; 9619 Information Related to Geologic Time: Precambrian; 1025 Geochemistry: Composition of the mantle; *KEYWORDS:* lithosphere, surface wave, Baltic Shield

**Citation:** Bruneton, M., et al. (2004), Complex lithospheric structure under the central Baltic Shield from surface wave tomography, *J. Geophys. Res.*, 109, B10303, doi:10.1029/2003JB002947.

<sup>1</sup>Laboratoire de Géophysique Interne et Tectonophysique, Observatoire des Sciences de l'Univers de Grenoble, Grenoble, France.

<sup>2</sup>Temporarily at GeoForschungsZentrum Potsdam, Potsdam, Germany.

<sup>3</sup>Département de Sismologie, Institut de Physique du Globe de Paris, Paris, France.

<sup>4</sup>Laboratoire de Géodynamique des Chaînes Alpines, Observatoire des Sciences de l'Univers de Grenoble, Grenoble, France.

<sup>5</sup>Laboratoire de Planétologie et Géodynamique, Université de Nantes, Nantes, France.

<sup>6</sup>Ecole et Observatoire des Sciences de la Terre, University of Strasbourg, Strasbourg, France.

<sup>7</sup>GeoForschungsZentrum Potsdam, Potsdam, Germany.

<sup>8</sup>Institute of Geophysics, ETH Zurich, Zurich, Switzerland.

<sup>9</sup>Deceased.

<sup>10</sup>Institute of Geophysics, University of Stuttgart, Stuttgart, Germany.

<sup>11</sup>Institute of Geophysics, Warsaw University, Warsaw, Poland.

<sup>12</sup>Institute of Geophysics, Department of Seismology, Polish Academy of Sciences, Warsaw, Poland.

<sup>13</sup>Institute of Seismology, University of Helsinki, Helsinki, Finland.

<sup>14</sup>Department of Geophysics, University of Oulu, Oulu, Finland.

<sup>15</sup>Institute of Physics of the Earth, Russian Academy of Sciences, Moscow, Russia.

<sup>16</sup>Department of Earth Sciences, Utrecht University, Utrecht, Netherlands.

<sup>17</sup>Geophysical Institute, Academy of Sciences of the Czech Republic, Prague, Czech Republic.

<sup>18</sup>Department of Earth Sciences, University of Uppsala, Uppsala, Sweden.

<sup>19</sup>Kola Scientific Center, Russian Academy of Sciences, Apatity, Russia.

<sup>20</sup>Sodankylä Geophysical Observatory Oulu Unit, University of Oulu, Oulu, Finland.

<sup>21</sup>Spezgeofisika MNR, Moscow, Russia.

## 1. Introduction

[2] The formation and evolution of the earliest continents remain an enigma in Earth sciences. The development of thick lithospheric roots seems to have protected the continental crust from recycling into the mantle. The vertical and lateral extent of these keels and the timing of the stabilization remain unknown. To understand these problems further requires a more complete understanding of the structure of the cratonic lithosphere and the relationship between the crust and upper mantle. Studies of mantle xenoliths can provide insight into the composition and age of the mantle, while seismic studies provide information on the lateral extension of the heterogeneities. For example, *James et al.* [2001] show beneath the Kaapvaal and Zimbabwe cratons in South Africa that thick roots are confined to the Archean cratons with no evidence of similar structures beneath the adjacent Proterozoic mobile belts. This is in good agreement with the age distribution of mantle xenoliths proposed by *Pearson et al.* [2002].

[3] The Fennoscandian Shield is the northwestern crustal segment of the East European Craton. It is formed by an Archean nucleus, the Karelian province, flanked to the northeast by the late Archean-Paleoproterozoic Lapland-Kola mobile belt and to the southwest by the Proterozoic Svecofennian domain [*Gorbatshev and Bogdanova*, 1993]. The formation of the granite-greenstone Karelian province started some 3.5 Gyr ago and continued through the Archean with orogenic maxima around 2.9 and 2.7 Ga [*Gorbatshev and Bogdanova*, 1993]. The growth of continental crust continued with the accretion of several lithospheric blocks over a very long time span through the late Archean and Proterozoic. The formation of the Svecofennian domain was first thought to be very simple and homogeneous, but recently, *Nironen et al.* [2002] proposed a succession of five orogenies between 1.92 and 1.79 Ga alternating with continental extensions. The last recorded tectonic events are extensional with the intrusion of the Rapakivi granitoids (1.65–1.54 Ga) and the sedimentation of the Subjotnian sandstone formation (1.2 Ga) [*Korja et al.*, 1993]. Since that time the central part of the shield has remained stable.

[4] This composite craton, uncovered by sediments, without noticeable reworking since 1.2 Ga is an ideal place to test the differences between Archean and Proterozoic lithospheres. This area was therefore chosen for one of the investigations of the EUROPROBE program [*Gee and Zeyen*, 1996], namely, the Svecofennian-Karelia-Lapland-Kola (SVEKALAPKO) project [*Hjelt and Daly*, 1996]. Part of the SVEKALAPKO project was a teleseismic experiment covering the Finnish part of the Svecofennian domain and southern Karelian province [*Bock and the SVEKALAPKO Seismic Tomography Working Group (SSTWG)*, 2001]. This array was designed to study the lithosphere-asthenosphere system of the central Baltic Shield and especially the boundary between the Proterozoic Svecofennian domain and the Archean Karelia. The results of regional teleseismic *P* wave tomography using the SVEKALAPKO data set shows a central positive velocity anomaly that can be traced to a depth of 300 km, located in the area of the contact between the Archean and Proterozoic domains. This model does not support the idea of a simple change in lithospheric

structure associated with the Archean-Proterozoic boundary [*Sandoval et al.*, 2004].

[5] Previous seismic studies of the Baltic Shield have yielded very different estimates of the lithospheric thickness, varying between 160 and 350 km [*Sacks et al.*, 1979; *Husebye and Hovland*, 1982; *Calcagnile*, 1982; *Babuška et al.*, 1988; *Calcagnile*, 1991]. These studies base their conclusions on different concepts, low-velocity zone, wave conversion, lack of lateral heterogeneities, that do not refer to the same physical interpretation of the lithosphere-asthenosphere boundary so they are not necessarily compatible.

[6] The SVEKALAPKO seismic tomography experiment is a unique opportunity to obtain the absolute shear wave velocities in the upper mantle in Fennoscandia through surface wave analysis. We use a new tomography technique, developed by *Bruneton et al.* [2002]. This method is based on two-dimensional ray tracing and takes into account the nonplanarity of incoming wave fronts. Travel times are inverted to obtain phase velocity maps of the area. One advantage of this surface wave tomography is that the receivers are located within the tomographic model and not at the model edge as is the case in body wave tomography, which allows an efficient modeling of the shape of incoming wave fronts in terms of arrival time on the edge of the study area.

## 2. Data Selection and Processing

[7] Between August 1998 and May 1999 more than 140 seismic stations operated in the framework of the SVEKALAPKO project [*Bock and SSTWG*, 2001]. The network was deployed on a two-dimensional grid covering the central part of the Fennoscandian Shield in southern Finland. Out of these stations, 46 were equipped with broadband sensors (CMG3 and STS2, cutoff period 90–100 s; CMG40, cutoff period 40–60 s). Very good recording conditions in the shield made it possible to analyze surface waves with periods up to 190 s. Figure 1 shows the locations of the broadband stations as well as the main tectonic features.

[8] For the present study we use the fundamental mode Rayleigh wave recorded on the vertical component of the sensors. Because of the large number of different sensors and recorders, the data are first corrected for the instrument response. Then we use a phase-matched filter [*Herrin and Goforth*, 1977; *Lander and Levshin*, 1989] to extract the fundamental mode Rayleigh wave from the signal.

[9] Out of all the recorded earthquakes of magnitude higher than 5.5 and epicentral distance larger than 30°, we select 69 events showing a high-quality signal at most of the stations. The geographic distribution of these events is shown in Figure 2. On the filtered signals we measure time delays between pairs of stations versus frequency using the phase of the Wiener filter [*Wiener*, 1949; *Hwang and Mitchell*, 1986; *Cotte et al.*, 1999]. For each station pair we eliminate frequency points with a coherency lower than 0.95 or a signal-to-noise ratio lower than 4. The value of the threshold is chosen from the result of numerical tests using full waveform synthetic seismograms: the recovered veloc-

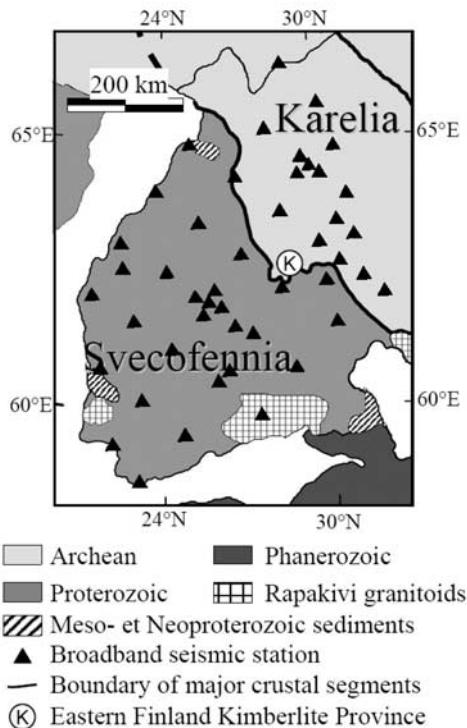


**Figure 1.** Simplified geological map of the central Baltic Shield (modified from *Hjelt and Daly [1996]*). Triangles give the location of the broadband stations of the SVEKALAPKO array. The location of the Eastern Finland Kimberlite Province is marked with the letter K.

ities remain close to the input model with a signal-to-noise ratio down to 3.5 [*Bruneton et al., 2002*].

[10] The data we need in the inversion for phase velocity under the station array (see section 3) are arrival times of the fundamental mode Rayleigh wave at every station for each event and period. The simplest way to convert our delay times into arrival times is to set the origin time for each event to be the arrival time at one station chosen as the reference and to use arrival times relative to this particular station.

[11] For each event the reference station is chosen as one with a very high quality signal out of the first stations encountered by the wave. As a stabilization procedure we consider as arrival time for a given station the mean of all available time delay measurements with the reference station using an intermediate third station. For example, for a given event and period for which  $n$  stations (out of which one is the reference station) have high-quality signals. The time delay between any station and the reference station is an average of  $n - 1$  delay values: one is measured directly with the reference station,  $n - 2$  other estimations are the sum of the delay between the particular station and a third station and the delay between the third station and the reference.

[12] Our estimation of the uncertainty associated with the final arrival time is twice the standard deviation of the  $n - 1$  times used to obtain the delay. This rather pessimistic value is used because the different measurements are not inde-

pendent, so we consider one standard deviation to be a too optimistic error estimate. For a better consistency of the data set we also impose a minimum value of 1 s for the uncertainty. We assume the data to be uncorrelated, and consequently, the data covariance matrix is a diagonal matrix containing the squared uncertainties.

### 3. Inversion for Phase Velocity Maps

[13] To obtain a three-dimensional model in shear wave velocity for the region underneath the array, we adopt a two-step method. The first step consists in inverting propagation times of the fundamental mode Rayleigh wave to compute phase velocity maps at each frequency. The combination of the different maps obtained for different frequencies gives a dispersion curve at each location on the map. The second step is an inversion of the dispersion curves to obtain shear wave velocity versus depth mapping at each grid node and consequently a three-dimensional (3-D) shear wave velocity model. This approach, justified by the good azimuth and epicentral distance distribution of the events (see Figure 2), is based on the assumption that the phase velocity maps yield the structural velocity as defined by *Wielandt [1993]*. The structural velocity corresponds to the phase velocity in hypothetical flat-layered models with the same elastic parameters as the medium immediately below the considered point.

[14] To invert the travel times obtained at a given frequency for a phase velocity map, we use the method recently developed by *Bruneton et al. [2002]*. It is derived from two main ideas: (1) the use of phase information which is more robust than the amplitude and (2) the necessity to take into account the nonplanarity of wave fronts for surface wave studies [*Tryggvason, 1961; Friederich et al., 1994*]. Here we only recall the main characteristics of the method;

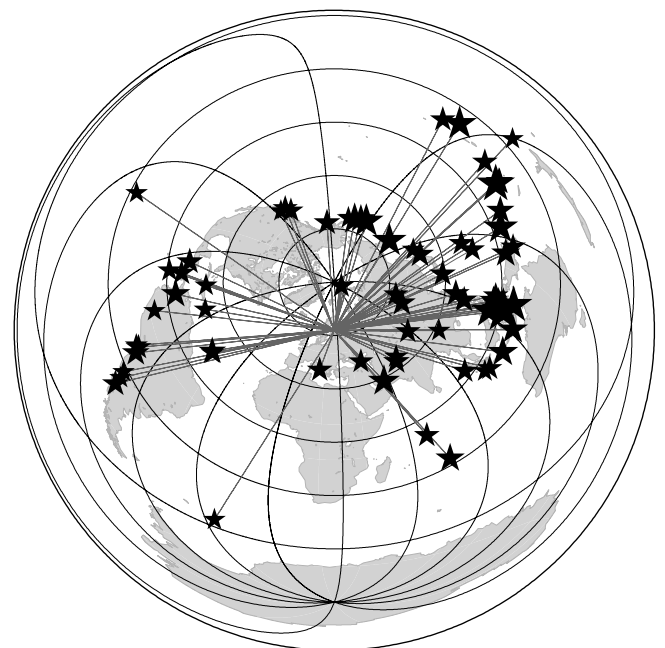


**Figure 2.** Distribution of the 69 events selected for this study. The size of each star is proportional to the magnitude of the event.

for a more detailed description we refer to *Bruneton et al.* [2002].

### 3.1. Forward Problem and Boundary Conditions

[15] The calculation of the travel times is based on the eikonal equation

$$(\nabla T)^2 = c^{-2} = u^2, \quad (1)$$

where  $T$  is the arrival time of the wave,  $\nabla$  is the horizontal gradient,  $c$  is the phase velocity, and  $u$  is the slowness of the medium. The boundary conditions used in the forward problem derive from two hypothesis: (1) the ray goes through the receiver position  $\mathbf{x}_r$  and (2) the ray connects to the curved wave front at the edge of the study region. The wave fronts are modeled by arrival times  $T_0(x_i)$  of the wave along the edge of the study region. The projection of the slowness vector  $\mathbf{p}$  of the ray on the edge  $x_i$  should therefore be equal to the derivative of the arrival times  $\partial T_0/\partial x_i$ .

[16] The search for the ray that obeys the boundary conditions is done following a first-order perturbation technique known as paraxial ray theory [*Deschamps*, 1972; *Farra and Madariaga*, 1987]. Once the ray following all boundary conditions is traced, the arrival time of the wave at the receiver is computed by integration along the ray. The derivatives of the arrival time with respect to the model parameters are also computed [*Bruneton et al.*, 2002].

### 3.2. Inverse Problem

[17] The model  $\mathbf{m}$  of the inversion contains two types of parameters. The phase velocity field is modeled by slowness squared, parameterized using third-order two-dimensional B spline functions [*De Boor*, 1978] with coefficients distributed on grid nodes every 40 km in  $x_1$  and  $x_2$ . Each wave front is described by its arrival time at the two edges of the study region that are first encountered by the wave. Along each one of the two edges the arrival time is modeled using fourth-order B spline interpolation with grid nodes every 40 km. The node spacing of 40 km is chosen as a compromise between the ratio of number of parameters over number of data and the spatial resolution.

[18] Following *Bruneton et al.* [2002], the inverse problem consists in the minimization of a least squares misfit function  $S$

$$S(\mathbf{m}) = [\mathbf{T}^{\text{obs}} - \mathbf{T}^c(\mathbf{m})]^T \mathbf{C}_T^{-1} [\mathbf{T}^{\text{obs}} - \mathbf{T}^c(\mathbf{m})] + [\mathbf{F}_m - \mathbf{F}(\mathbf{m})]^T \mathbf{C}_F^{-1} [\mathbf{F}_m - \mathbf{F}(\mathbf{m})]. \quad (2)$$

The first part of equation (2) corresponds to the time residuals between observed  $\mathbf{T}^{\text{obs}}$  and calculated  $\mathbf{T}^c$  arrival times. The residuals are weighted by the uncertainty of each observation as described in the covariance matrix  $\mathbf{C}_T$ . As data are assumed to be uncorrelated, the nondiagonal terms of  $\mathbf{C}_T$  are set to zero. The diagonal terms contain the variance of each data element (see the end of section 2). Introduction of nondiagonal data covariance terms in the inversion may slightly modify the a posteriori error in the model parameters, but this effect

is negligible compared to the effect of the smoothing constraints.

[19] Additional information is needed due to the non-unicity of the solution. The second part of equation (2) therefore corresponds to the introduction of a priori information.  $\mathbf{F}_m$  is the a priori value of some parameter combination  $\mathbf{F}(\mathbf{m})$ . The uncertainty of the a priori value is described through the diagonal terms of the covariance matrix  $\mathbf{C}_F$  of the a priori constraints. Ideally,  $\mathbf{C}_F$  should directly reflect the resolution that we can expect to obtain on the various parameters that we invert for. Section 3.3 therefore focuses on resolution tests, and section 3.4 describes a priori conditions used as well as their effect on the obtained model.

[20] The nonlinear least squares equation (2) can be solved iteratively by a Gauss-Newton method. The functions  $\mathbf{T}^c(\mathbf{m})$  and  $\mathbf{F}(\mathbf{m})$  are linearized around a starting model  $\mathbf{m}_0$  to obtain the quadratic approximation of the misfit function  $S$ . For each period,  $\mathbf{m}_0$  is composed of a homogeneous phase velocity and of plane wave fronts incident from the back azimuths determined for each event by fitting a plane wave to the arrival times at all stations. The phase velocity for each period derives from a 1-D inversion of the data set [*Bruneton et al.*, 2004]. Several other starting phase velocities have been tested, in particular, the one calculated for the standard Earth model ak135 [*Kennett et al.*, 1995]; the phase velocities recovered are always similar to the one presented.

[21] As described by *Bruneton et al.* [2002], the quadratic approximation is solved using a singular value decomposition algorithm. As the problem is nonlinear, the process is repeated until the misfit function stops decreasing. Using the SVEKALAPKO data set, the final model was generally obtained after two iterations, indicating that the nonlinearity of the problem is weak.

[22] In the inversion for phase velocity maps the a posteriori covariance matrix of the model is computed following *Tarantola* [1987] [see also *Bruneton et al.*, 2002, equation 17]. This error estimate varies as a function of several factors: the experiment geometry and the volume of data, the covariance matrix of the travel time data (see section 2), and the a priori uncertainty chosen for the a priori constraints. The strength of the a priori constraints therefore has to be carefully chosen (see section 3.4).

[23] The a posteriori variance of the slowness squared  $\sigma_{u^2}$  can be converted into the variance of the phase velocity  $\sigma_c$  by differentiation of  $u^2 = c^{-2}$ :

$$\sigma_c = c^3 \sigma_{u^2} / 2. \quad (3)$$

To be able to compare the phase velocity uncertainties for different frequencies, we use a constant reference phase velocity  $c = 4 \text{ km s}^{-1}$  in equation (3).

### 3.3. Resolution Assessments

[24] A large set of resolution tests has been applied to the method using synthetic data computed from direct ray tracing and full waveform modeling [*Bruneton et al.*, 2002]. The method is very robust in determining phase velocity maps in all synthetic examples. The tests show that structures larger than 150 km under the SVEKALAPKO broadband array are well resolved. The use of arrival times

restrains us to structures of sizes bigger than the wavelength for each period. The domain of validity of ray theory has been shown to be generally more restrictive [see, e.g., *Spetzler et al.*, 2002], but *Bruneton et al.* [2002] showed that in the setting of the SVEKALAPKO seismic experiment, structures of size similar to the wavelength are also recovered by the inversion. This estimate is of the same order as the influence zone used by *Kennett and Yoshizawa* [2002] or the resolution scale computed by *Friederich* [2003] in regional surface wave tomographies.

### 3.4. A Priori Constraints

[25] We use five types of a priori conditions; each of them is represented by an equation and should reflect the model resolution. The chosen value for each uncertainty gives the strength of the constraint and depends on how tightly we want it to be followed by the model; that is, they should reflect the resolution on the model.

[26] The absolute value of the velocity (condition 1) is assumed to be close to an a priori value for each period within an uncertainty  $\sigma_{F_{u^2}}$  expressed in  $\text{s}^2 \text{ km}^{-2}$  as the model parameters representing the velocity are slowness squared. We choose

$$\sigma_{F_{u^2}} = 5 \times 10^{-3} \text{ s}^2 \text{ km}^{-2}, \quad (4)$$

allowing variations of less than  $\pm 4\%$  in velocity. This choice is based on the results of *Sandoval et al.* [2004], who show  $P$  wave velocity variations of up to 2%. Even though we can expect stronger variations in  $S$  than in  $P$  wave velocity, there is no reason to expect very strong  $S$  wave velocity variations related to, for example, partial melt.

[27] The travel time of a wave is sensitive to the structure located in the Fresnel zone of the ray. As we compute the partial derivatives by simple integration along the ray, we decide to take this property into account by an a priori smoothing of the medium. Therefore the first (condition 2) and the second (condition 3) derivatives of the slowness squared with regard to the horizontal coordinates are assumed to be close to zero within respective uncertainties  $\sigma_{F_{dx^2}}$  and  $\sigma_{F_{d^2u^2}}$ :

$$10^{-5} \leq \sigma_{F_{dx^2}} \leq 5 \times 10^{-4} \text{ s}^2 \text{ km}^{-3}, \quad (5)$$

$$10^{-7} \leq \sigma_{F_{d^2u^2}} \leq 2 \times 10^{-6} \text{ s}^2 \text{ km}^{-4}, \quad (6)$$

$\sigma_{F_{dx^2}} = 3 \times 10^{-4} \text{ s}^2 \text{ km}^{-3}$  represents up to 5% velocity variation over a distance of 20 km. The constraint on the second derivative ( $\sigma_{F_{d^2u^2}}$ ) is more subtle. It corresponds to restricting the variations of the velocity gradient (or the number of maxima and minima) to reduce fluctuating solutions. As the size of the Fresnel zone increases with increasing wavelength, the values of  $\sigma_{F_{dx^2}}$  and  $\sigma_{F_{d^2u^2}}$  decrease linearly with increasing wavelength.

[28] The wave fronts are modeled by arrival times on the two edges of the study region first encountered by the wave, the two edges being treated independently. The times  $T_0$  (condition 4) corresponding to the same point on the two

edges are forced to be identical within a small uncertainty, allowing for small errors due to delay time measurements:

$$\sigma_{F_T} = 0.1 \text{ s}. \quad (7)$$

[29] A smoothness criterion for the wave front (condition 5) is added by identifying the derivative of the arrival time  $T_0$  along the boundary to that of a plane wave arriving from the back azimuth  $\phi$ :

$$\frac{\partial T_0}{\partial x_1} = -\frac{\sin \phi}{c} \quad \text{or} \quad \frac{\partial T_0}{\partial x_2} = \frac{\cos \phi}{c}, \quad (8)$$

where the axes  $x_1$  and  $x_2$  are oriented toward the east and south, respectively. This criterion is motivated by the wave front healing process that tends to erase small-scale wave front variations [*Nolet and Dahlen*, 2000]. In this study, the angle  $\phi$  is determined for each event by fitting a plane wave to the arrival times of the given wave front at all stations for each frequency. The uncertainty is taken as

$$\sigma_{F_{dt}} = 5 \times 10^{-2} \text{ s km}^{-1} \quad (9)$$

allowing at least  $10^\circ$  variations in the propagation direction (the exact value depends on the angle between the back azimuth and the edge of the box considered).

[30] The influence of the different constraints on the resulting phase velocity maps was widely tested on the data. The most important effect is due to the smoothing constraint: depending on the value we use for  $\sigma_{F_{dx^2}}$  and  $\sigma_{F_{d^2u^2}}$ , the granularity of the solution and to a lesser extent the amplitude of the anomalies change. However, the main features of the phase velocity maps remain stable. We therefore set the constraints to the above values, so that the obtained model fulfills the considerations discussed above: (1) the minimum size of a resolved structure is 150 km, and (2) the smallest structure resolved by a given seismic wave has the size of its wavelength. The a posteriori variance in the model parameters mainly depends on these two a priori conditions, revealing that small-scale structures are sensitive to noise.

[31] The increase of the constraints on the lateral variations with the wavelength corresponds to a smaller number of independent parameters. The velocity values are therefore well resolved at long periods which corresponds to small a posteriori errors. However, these small errors at long periods do not reflect reality: even though the velocities are well resolved in a mathematical sense, there may still be significant lateral variations of structural velocities at long periods. To obtain more realistic error measurements, we add a constant uncertainty to the velocity errors so that the maximum uncertainty is the same for all periods. The reference period for this normalization is taken as 20 s. Figure 3 shows the a posteriori error in the phase velocity obtained for periods between 15 and 100 s.

### 3.5. Phase Velocity Model

[32] Figure 4 presents the phase velocity maps obtained for periods between 15 and 100 s. The most prominent feature is a slow structure in the center of the array for the higher frequencies. Its position and shape correspond

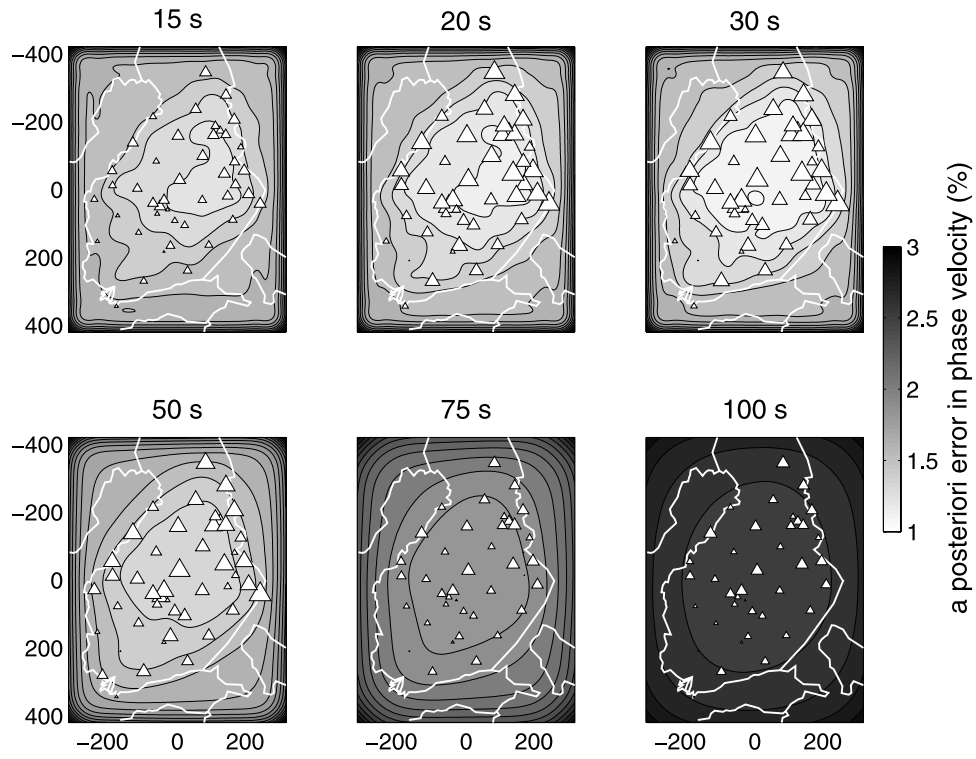


**Figure 3.** A posteriori error in the phase velocity for different periods. Triangles represent the station position, and their size is proportional to the volume of data recorded for the given station and period.

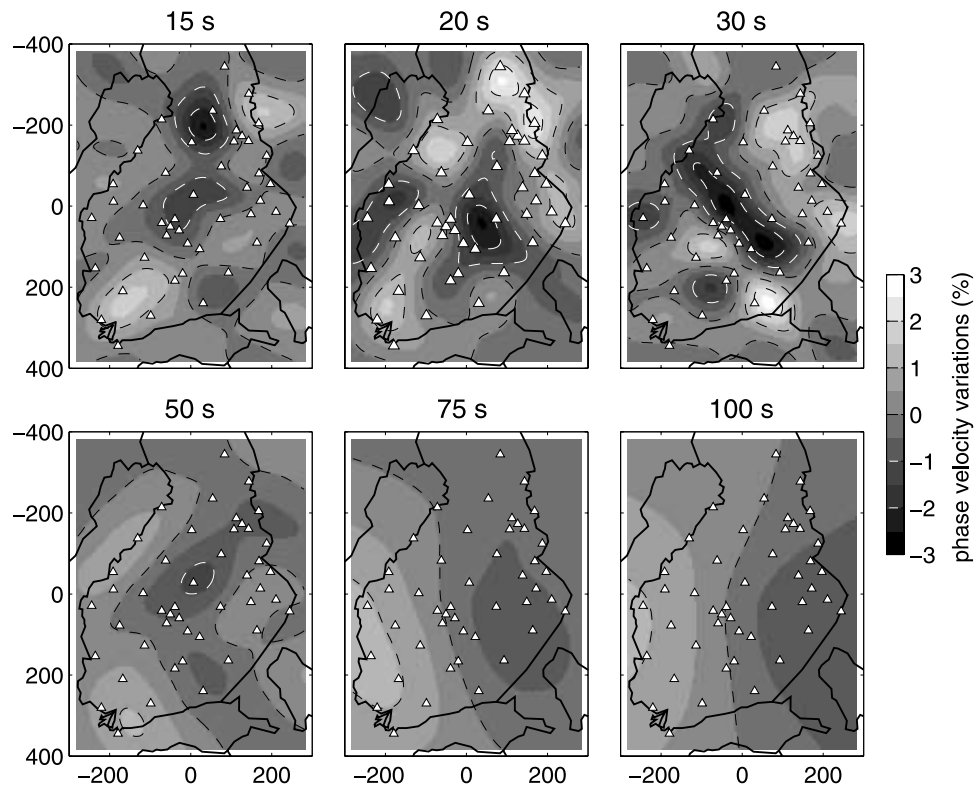


**Figure 4.** Lateral variations of the phase velocity for selected periods of the fundamental mode Rayleigh wave in percentage of the average value for the period (15 s,  $3.44 \text{ km s}^{-1}$ ; 20 s,  $3.56 \text{ km s}^{-1}$ ; 30 s,  $3.85 \text{ km s}^{-1}$ ; 50 s,  $4.08 \text{ km s}^{-1}$ ; 75 s,  $4.20 \text{ km s}^{-1}$ ; and 100 s,  $4.29 \text{ km s}^{-1}$ ). Triangles mark the station locations.

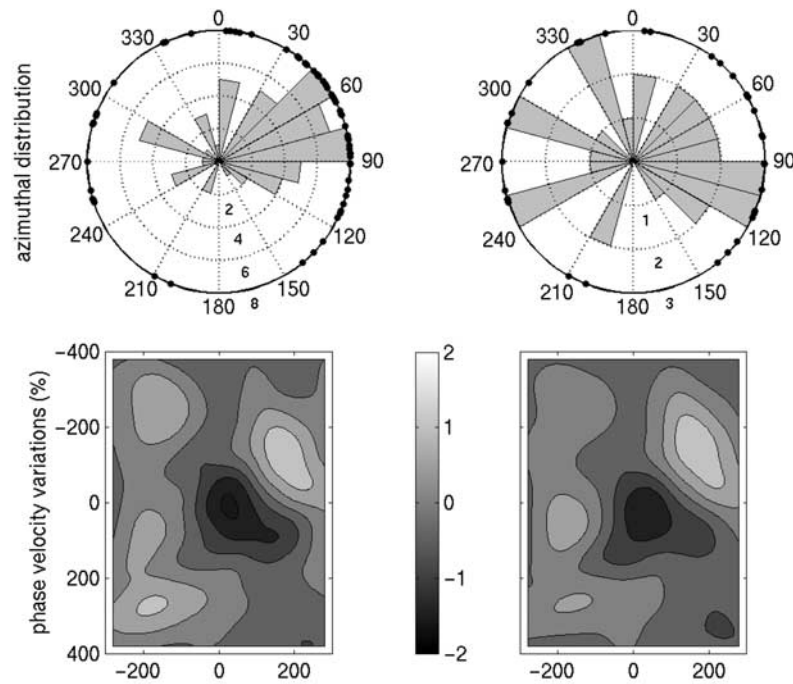


**Figure 5.** Influence of the azimuth distribution on the phase velocity map, example for 40 s period. (left) Complete data set and (right) reduced data set with an almost uniform azimuth distribution.

roughly with the deep Moho structure imaged by *Sandoval et al.* [2003].

[33] The reduction of the misfit function is always important and is mainly due to the curvature of the wave fronts. At short (<30 s) and long (>100 s) periods the final misfit function is larger than 1, indicating that the theory used does not completely explain the data within the error bars. This may be due to a high noise level at some stations or to phenomena we do not take into account in our modelization, for example, anisotropy and diffraction.

[34] The azimuth distribution of our data is not perfect as a majority of events are located in the northeastern quarter. To test the influence of the azimuth distribution, we remove some events of our data set to obtain a maximum of two events per 15° sector in the northeastern quarter and three events elsewhere. The events selected are those with the best fit to a plane wave as this ensures that only highest-quality events are selected: a bad fit to the plane wave could correspond to questionable measurements or to an anomalous wave front that we cannot model using ray theory.

[35] Figure 5 shows an example for the period of 40 s, the azimuth distribution of the complete and reduced data sets are plotted in Figure 5 (top), and the associated phase velocity map is given in Figure 5 (bottom). The two phase velocity maps are very similar. The position and shape of the heterogeneities are not modified with a better azimuth distribution except for an effect of smoothing; their amplitude is also slightly reduced. Both reduction and smoothing are explained by the fact that the values of the constraints are identical for the two inversions. As the volume of data is reduced in the second data set the relative importance of the smoothing constraints is larger.

[36] The same conclusion is drawn for all the periods used in this study. As was already noticed by *Bruneton et al.*

[2002], the azimuth distribution does not have an important effect on the inversion result for the SVEKALAPKO array.

#### 4. Inversion for 3-D Shear Wave Velocity Model

[37] As output of the previous inversion we obtain phase velocity maps for a series of periods. At every location in the study region this is equivalent to a phase velocity dispersion curve. Figure 6 presents all dispersion curves

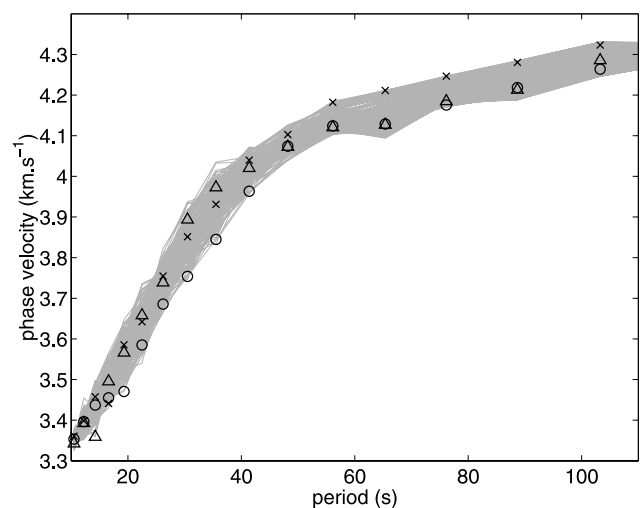


**Figure 6.** Fundamental mode Rayleigh wave phase velocity dispersion curves. Each grey line represents the obtained dispersion for one location on the map, three of them from the northeastern (triangles), central (circles), and southwestern (crosses) parts of the array have been highlighted with symbols.

obtained in the central part of the study region, out of which three are highlighted. We invert independently each of these curves for a shear wave velocity versus depth profile ( $V_s(z)$ ) associated to each grid node on the map.

#### 4.1. Inversion of the Dispersion Curves

[38] This inversion follows a linearized method that allows the consideration of both independent layers and continuous media between the interfaces [Maupin and Cara, 1992]. For the direct modeling and computation of the partial derivatives we use the program package developed by Saito [1988]. The inversion algorithm is that of Tarantola and Valette [1982], minimizing the square of the phase velocity discrepancy. The  $P$  wave velocities and densities are kept constant during the inversion. The influence of these two parameters on the inversion is small. Using, for example, constant Poisson ratio produces a similar  $S$  wave velocity model.

[39] The initial model used for the 3-D inversion is obtained by inversion of an average dispersion curve for the whole modeled area. The average dispersion curve derives from the procedure described in section 3, using a unique cell covering the stations array but enabling curved wave fronts. The inversion for shear wave velocity with depth of this average dispersion curve is done using a large correlation length in order to obtain a well-constrained average model. The initial model for this preliminary inversion derives from smoothing of the standard Earth model ak135 [Kennett et al., 1995] for the mantle part. The crustal structure follows the compilation of deep seismic sounding profiles by Sandoval et al. [2003], containing a high-velocity lower crust and a Moho depth of 51 km. For a more detailed discussion of the average model, see Bruneton et al. [2004].

[40] In the algorithm of Tarantola and Valette [1982] the use of a model covariance matrix makes it possible to quantify the smoothness of the shear wave velocity with depth. The shape of the correlation functions is chosen to be Gaussian following Lévêque et al. [1991]. The correlation length is defined as the half width of the Gaussian for the 60% confidence interval.

[41] In the inversion of the dispersion curves the velocities obtained for the lower crust and shallow mantle are influenced by the chosen Moho depth. In the region of the SVEKALAPKO array the crustal structure is particularly well known because of numerous deep seismic sounding profiles. A compilation of all refraction and reflection data for the region was recently performed by Sandoval et al. [2003] to compute a 3-D crustal model in  $P$  wave velocity. To constrain our dispersion curve inversions, we set the depth of the Moho discontinuity at every location following the Sandoval et al. [2003] Moho depth model. We also test the influence of the Moho depth on the obtained model.

[42] The result of our second inversion step is an absolute shear wave velocity model constructed from surface waves of wavelengths between 40 and 900 km. Because of anelasticity in the Earth such a model cannot be directly compared with velocities obtained from other techniques, short-period body wave tomography in particular. The velocity model we present here is corrected for anelasticity using a simple  $Q(z)$  model derived from the preliminary reference Earth model (PREM) [Dziewonski and Anderson,

1981] (adapted for each Moho depth) and a reference frequency of 1 Hz, so as to facilitate the discussion of our results. The correction is made according to equation (5.81) of [Aki and Richards, 2002]:

$$V(z)_{\omega_1} = V(z)_{\omega_2} \left[ 1 + \frac{1}{\pi Q(z)} \ln \left( \frac{\omega_1}{\omega_2(z)} \right) \right], \quad (10)$$

where  $\omega_1 = 1$  Hz and  $\omega_2(z)$  is a period representative of the periods of the surface waves that sample the medium at depth  $z$ . The use of a different  $Q$  model, within realistic limits, does not have a large influence on the result (for details, see Bruneton et al. [2004]).

#### 4.2. Shear Wave Velocity Uncertainty

[43] The dispersion curve inversion algorithm we use allows us to compute both the model a posteriori error bars and the resolution. These values depend on the phase velocity uncertainties obtained as described at the end of section 3.2 and on the a priori covariance of the  $S$  wave velocity model.

[44] The latter derives from an a priori error in shear wave velocity with respect to a reference model and a correlation length parameter. The a priori error in  $S$  wave velocity defines to what extent the final model can vary from the reference one; we choose a value of 4%. The reference model used is the same as the initial model described in section 4.1. Considering that it is an average model for the region, this value is relatively large and should allow all realistic phase velocity variations in the region. The correlation length defines the smoothness of the shear wave velocity model with depth. We choose a value of 20 km in the mantle, and we decorrelate crustal layers from the neighboring layers. An inversion with a smaller correlation length gives similar results (maximum discrepancy 0.2%) and confirms that our data do not contain information concerning the fine structure of the mantle.

[45] Figure 7 presents the obtained a posteriori standard deviation in shear wave velocity versus depth for three different locations. As the value at depth immediately below (above) an interface is correlated only with values at points below (above), the velocities in the neighborhood of interfaces are less constrained than inside the layer. This uncertainty is quite large at the Moho. The error increases with depth due to the larger error in the phase velocities for larger periods (see Figure 3).

[46] An estimation of the resolution of the lateral variations with depth can be computed from the penetration depth of the seismic wave used. We measure arrival times for periods between 10.5 and 190 s, which means that the wavelength varies between 35 and 900 km approximately. If the wavelength is larger than the aperture of the array, the lateral variations are not resolved. The deepest lateral variations that we can image are those recorded by the 100 s period Rayleigh wave of roughly 430 km wavelength. We therefore do not have any resolution in the lateral variations deeper than 150 km.

#### 4.3. The 3-D Shear Wave Velocity Model

[47] We first discuss the final 3-D shear wave velocity model and then show tests to estimate the influence of the initial model and of the Moho depth.

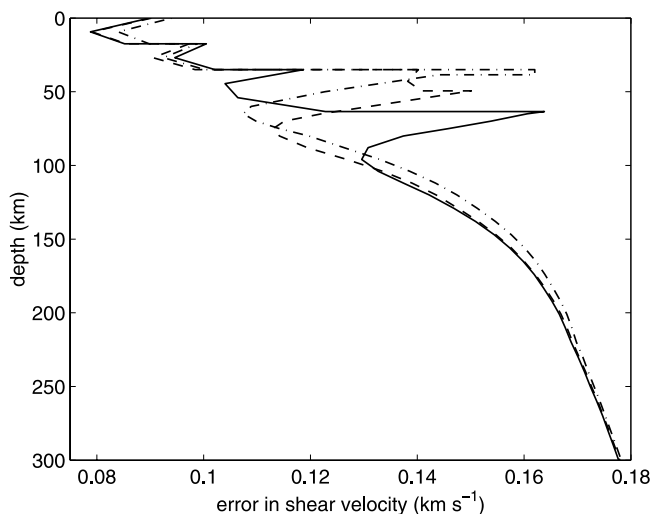


**Figure 7.** A posteriori error in shear wave velocity for three different Moho depths. Solid line corresponds to 63.5 km, dashed line corresponds to 49.5 km, and dash-dotted line corresponds to 38.5 km.

[48] Shear wave velocity versus depth profiles (Figure 8) show that the region is characterized by, on average, a lithospheric mantle 4% faster than standard Earth models. The depth-averaged velocity does not exhibit a low-velocity zone (LVZ), while most of the individual profiles show a minor LVZ at depths between 140 and 240 km. We interpret these variations as lateral variations in the composition of the lithosphere and not as variations of the depth of the lithosphere-asthenosphere boundary (see section 5).

[49] The final three-dimensional model is presented in Figures 9 (horizontal slices) and 10 (vertical cross sections). We observe  $S$  wave velocity variations of  $\pm 3\%$ , which are compatible with  $P$  wave velocity variations of  $\pm 2\%$  [Sandoval *et al.*, 2004]. The shallower levels of the mantle are characterized by higher velocity in the center of the array than at the periphery, but this high-velocity anomaly does not correlate well with the location of the major Moho trough.

[50] From 120 km and deeper, lower velocities are observed in the northeastern part of the array and in a smaller spot in the southeast; higher velocities are situated mostly in the western part. The Archean-Proterozoic boundary is not associated with a clear pattern in the upper 150 km of the mantle. Below 100 km the Archean domain seems to be mainly associated with low relative velocities whereas the Proterozoic domain mainly has high velocities. This is not consistent with the classical model of a highly depleted Archean lithosphere with high velocities and a less depleted Proterozoic mantle with low relative velocities [Jordan, 1979].

#### 4.3.1. Influence of the Initial Model

[51] To test the influence of the initial model on the recovered 3-D shear wave velocity, we also use a second initial model, which derives from theoretical seismic velocities computed by Kukkonen *et al.* [2003] from xenolith compositions and an associated regional geotherm. The two initial models are very similar except for the lower crustal

layer where the velocity of the xenolith-derived model is lower by 1.5% and for the mantle above 90 km depth where the velocity is 1% higher. The change in the initial shear wave velocity does not influence the recovered lateral variations while the absolute values of the shear wave velocities are shifted by approximately the same amount as the initial model in the uppermost mantle. This uncertainty on the velocity immediately below the Moho was also illustrated in Figure 7. However, below 90 km depth, the shear wave velocity model do not depend on the initial model.

#### 4.3.2. Influence of the Moho Depth

[52] The procedure of inversion of the dispersion curve does not invert for the depths of interfaces in the crust and mantle. The constant Moho depth is a very strong constraint on the shear wave velocity model. We therefore test the effects of a reasonable modification of the Moho depth model.

[53] The 3-D crustal model used, based on active seismics [Sandoval *et al.*, 2003], has been tested by forward modeling of  $P$  and  $S$  wave arrivals of local events. A joint inversion of seismic and gravity data recently confirmed this crustal structure and supplemented it with density values [Kozlovskaya *et al.*, 2004]. The shape and depth of the Moho in the region of the SVEKALAPKO array are estimated to be precise within 2 km. Such a precise knowledge of the crustal structure is exceptional and provides important constraints for seismic studies of the mantle.

[54] For a point in the center of the array we conduct two inversions by varying the Moho depth by 3 km. The change in the Moho depth affects the recovered velocity of the lower crustal layer and of the mantle down to  $\sim 100$  km: the

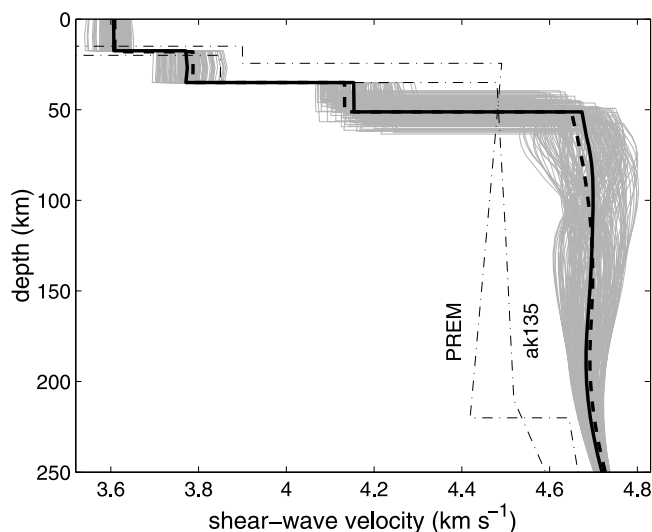


**Figure 8.** Shear wave velocity model with depth. Each grey line corresponds to an individual profile for a grid node. Solid black line corresponds to average model used as reference in Figures 9 and 10; dashed black line corresponds to initial model; thin dash-dotted lines correspond to standard Earth models PREM [Dziewonski and Anderson, 1981] and ak135 [Kennett *et al.*, 1995].

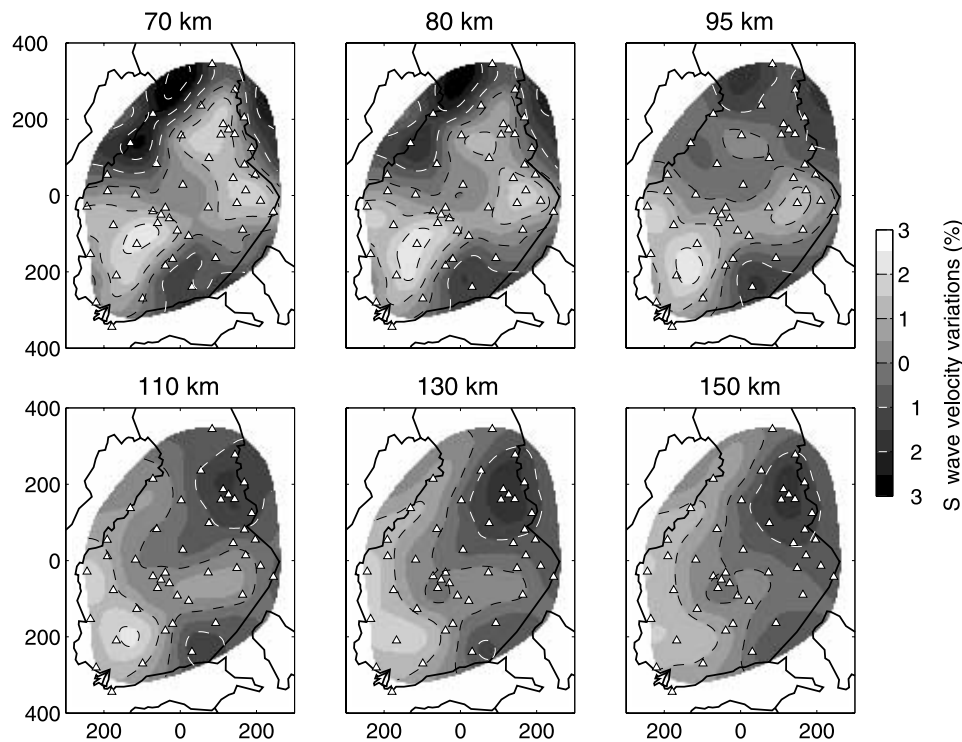


**Figure 9.** Horizontal sections at different depths in our 3-D shear wave velocity model. Lateral velocity variations are given in percentage with respect to the average velocity for the layer (70 km,  $4.66 \text{ km s}^{-1}$ ; 80 km,  $4.67 \text{ km s}^{-1}$ ; 95 km,  $4.68 \text{ km s}^{-1}$ ; 110 km,  $4.69 \text{ km s}^{-1}$ ; 130 km,  $4.70 \text{ km s}^{-1}$ ; and 150 km,  $4.69 \text{ km s}^{-1}$ ); triangles show the station positions.

deeper the Moho, the higher the upper mantle velocities. Variations are of the order of 0.75% for the crustal layer and  $<0.5\%$  for the mantle (see also the tests carried out by Bruneton *et al.* [2004]).

[55] The modifications of the velocity model produced by a 3 km modification of the Moho depth are half an order of magnitude lower than the lateral variations down to 80 km depth and decrease downward to zero at 100 km. Further improvements of the Moho map are unlikely to significantly modify our 3-D model.

## 5. Discussion

[56] Our 3-D shear wave velocity model is characterized by higher than average velocities in the lower crust and shallower mantle down to at least 100 km in the area where the Moho is anomalously deep. No clear pattern seems to be related to the surface geology, and in particular, the Archean and Proterozoic domains do not have significantly different velocities in the lithospheric mantle. The Baltic Shield appears more complex than the Kaapvaal craton in South Africa, where the higher lithospheric velocities are associated with the Archean domain and the lower lithospheric velocities are associated with the Proterozoic domain.

[57] For a further interpretation we made a semiautomatic classification of the  $V_s(z)$  curves. We first ran several automatic classifications using different criteria: depth of the minimum or maximum velocity, shape, and value of the velocity gradient. Then we selected the most efficient distribution into families: the one based on the depth of

the maximum velocity (between the Moho and 180 km depth). Six depth intervals were used in the automatic classification but only four of the six families had a geographically well defined core, independent of the exact boundaries of the depth intervals. The two remaining ones contained shear-wave velocity profiles with depth that were of generally different shapes or corresponding to points located in very distant areas. They were therefore subdivided into five “intermediate” families.

[58] Finally, once the nine families (four main and five intermediate) were defined, we visually inspected points geographically located on the limit between areas to ensure that any  $V_s(z)$  profile is associated with the family to which it resembled the most. Only very few points were moved from one family to the neighboring one.

[59] Figures 11a, 11c, 11g, and 11i show the main families, and Figures 11b, 11d, 11e, 11f, and 11h show the five intermediate families. If we compare our Figure 11j to the map of Plomerová *et al.* [2003] showing the pattern of anisotropy direction observed from  $P$  wave residuals, we can associate their Proterozoic family to our categories in Figures 11a, 11g, 11h, and 11i, their Archean family to our Figure 11c family, and their transitional region to our intermediate families in Figure 11d, 11e, and 11f. The two independent data sets agree on the existence of a region in the center of the SVEKALAPKO array characterized by a signature that seems to be intermediate between the Archean and the Proterozoic domains. However, the interpretation of the presence of the intermediate families could be due to the horizontal smoothing we apply during the inversion, to

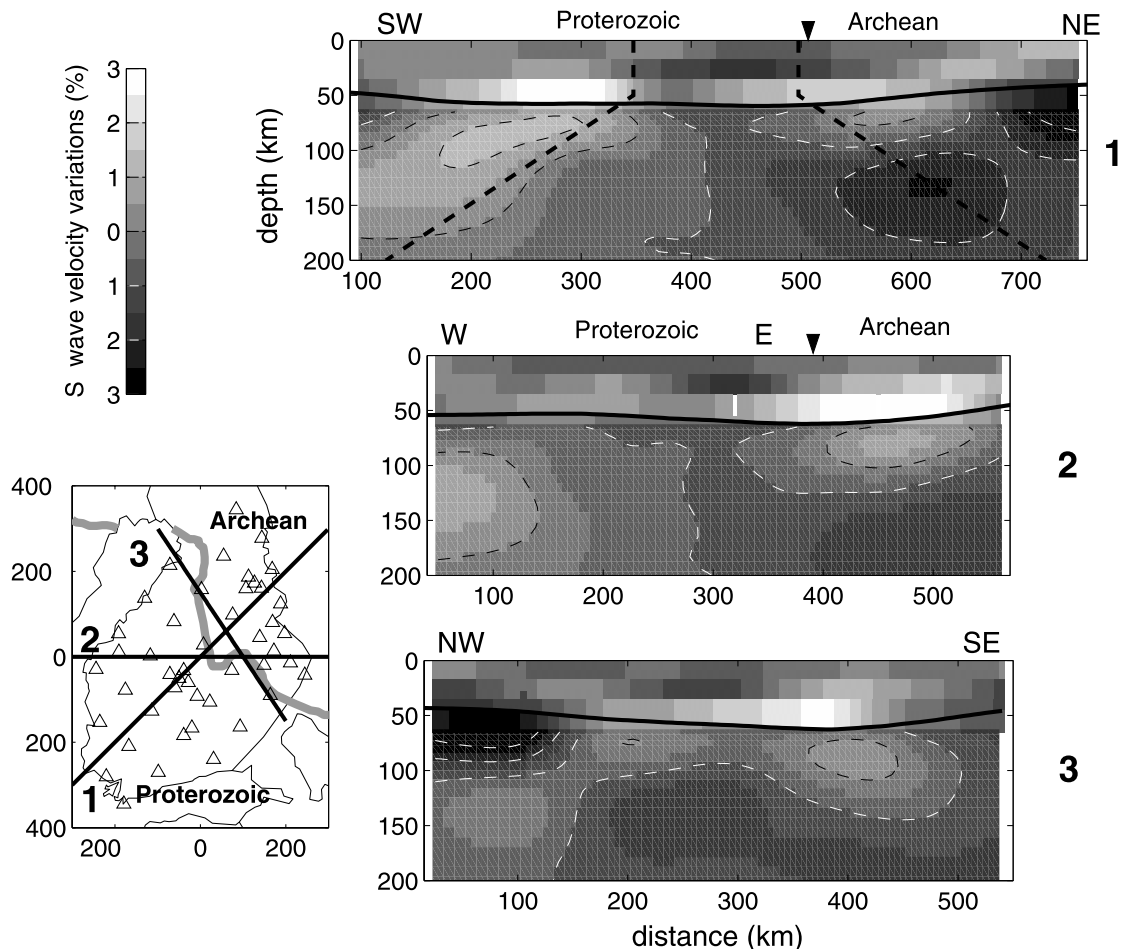


**Figure 10.** Vertical cross sections across the 3-D shear wave velocity model. (left) Map showing the location of the cross sections (thick black lines) numbered from 1 to 3 and the tectonic limit between Archean in the northeast and Proterozoic in the southwest (thick grey line). (right) Cross sections 1 to 3. Velocity variations are in percentage with respect to the average value for each depth. In sections 1 and 2 the inverted triangle indicates the approximate location of the tectonic Archean-Proterozoic boundary (section three approximately follows this boundary). The black line in the cross sections represents the Moho depth. The thick dashed lines of section 1 shows the lateral resolution length considered.

slanting transitions between the main families, or to different materials. We will therefore concentrate on the four main families, i.e., Figures 11a, 11c, 11g, and 11i.

[60] Interpretations of seismic velocity heterogeneities are generally based on thermal variations [see, e.g., Goes *et al.*, 2000; Röhm *et al.*, 2000].  $V_s$  variations of  $\pm 3\%$  over distances of a few hundred kilometers as observed in our model can be obtained with temperature variations of  $\sim 400$  K [Nataf and Ricard, 1996; Goes *et al.*, 2000]. However, this part of Fennoscandia shows no sign of any major thermal event for approximately the last 1.5 Gyr, a time that would be sufficient for the thermal conduction to erase temperature differences and smear out sutures between lithospheric blocks. Present measurements of the surface heat flow coupled with geochemical analysis of heat producing elements [Kukkonen, 1993], and integrated into a 2-D numerical thermal model of the lithosphere [Kukkonen and Jöeleht, 1996] support the idea of uniform upper mantle temperatures beneath Finland. This 2-D model also coincides with thermobarometric data on mantle xenoliths

in eastern Finland [Kukkonen and Peltonen, 1999; Kukkonen *et al.*, 2003]. The study of receiver functions shows horizontal interfaces at the seismic boundaries of 410 and 670 km [Alinaghi *et al.*, 2003], which also implies a homogeneous upper mantle temperature. Both interfaces are slightly shallower than the global average depth in the Earth, indicating a cold upper mantle. The cause of the observed seismic velocity variations must therefore be of compositional origin. On Figure 11, we show in black lines the velocity profiles derived from surface waves, and in grey lines the models computed from the mineral composition of “normal” peridotite sampled in the central Baltic Shield. We then propose a possible explanation for our four main families (Figures 11a, 11c, 11g, and 11i).

[61] The seismic velocities depend on the density and elastic parameters (compressibility and shear modulus), which in turn depend on the rock composition, the orientation of minerals, and the temperature and pressure conditions. The computations presented here follow the methodology explained by Goes *et al.* [2000]. We use

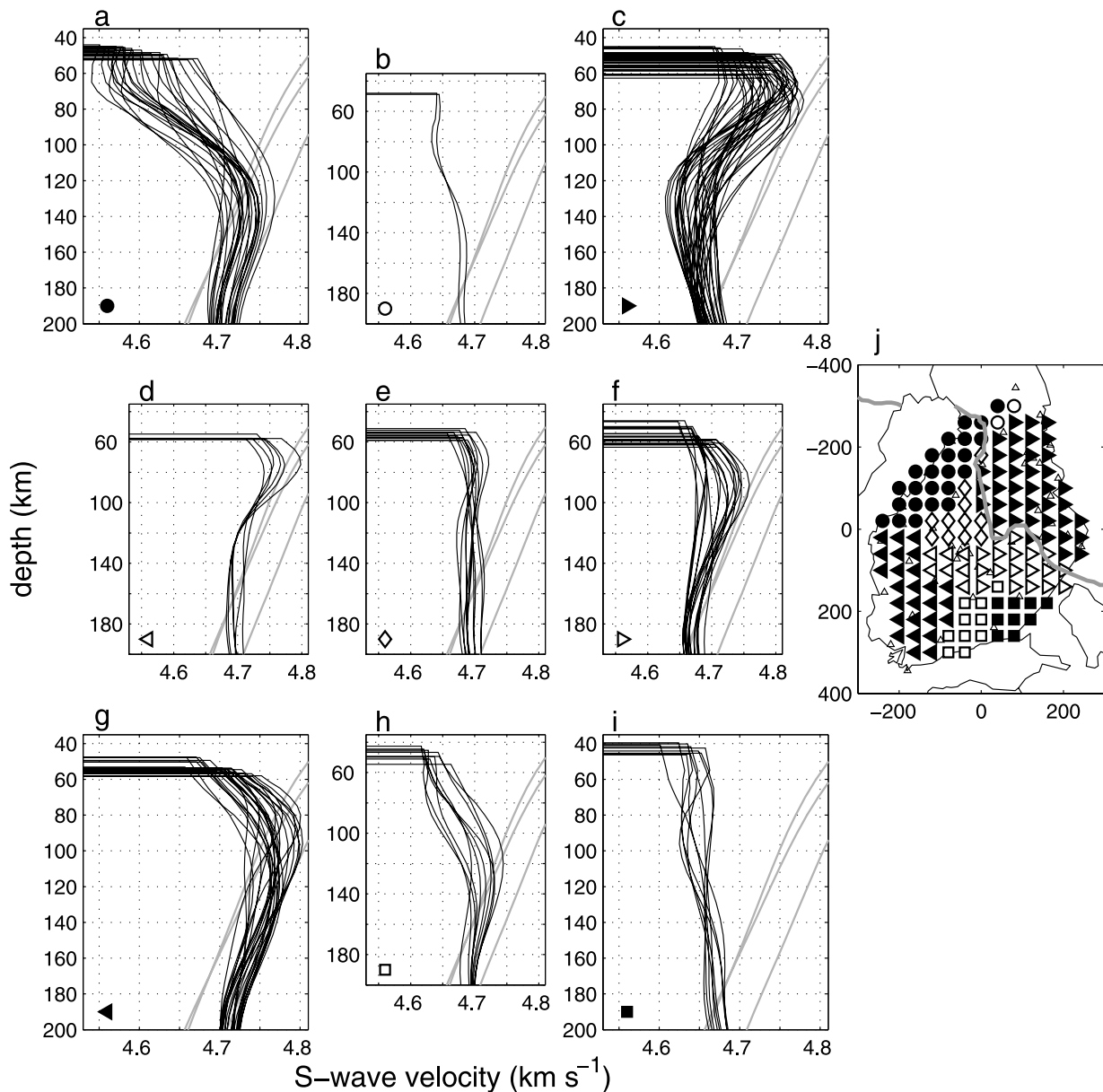


**Figure 11.** Classification of the shear wave velocity with depth profiles. (a–i) Black lines correspond to  $S$  wave velocity profiles, grey lines correspond to composition-based velocities, and the marker in the lower left corner refers to the marker on the map. (j) Map showing the location of the different families.

reference values for the density and elastic parameters of the major minerals as well as their pressure and temperature derivatives known from laboratory experiments [see *Goes et al.*, 2000, Table A1, and references therein]. The rock compositions used are lherzolite and harzburgite xenoliths, sampled in the eastern Finland kimberlite cluster (from lower to higher velocities: samples L66, L29, and L48 of *Kukkonen and Peltonen* [1999]). These kimberlites are situated in the Karelian Archean domain close to the boundary with the Svecofennian domain (see Figure 1). The origin depths of these particular samples as given by thermobarometry lie between 175 and 215 km [*Kukkonen and Peltonen*, 1999; *Kukkonen et al.*, 2003], but we computed the theoretical seismic velocities that would result

from the presence of these mineral compositions in the entire depth range studied. The regional geotherm used has been computed by *Kukkonen et al.* [2003]. It is calculated from a two-dimensional numerical thermal model of the lithosphere along a transect crossing the kimberlite province, combined with thermobarometric data on mantle xenoliths [*Kukkonen and Jöeleht*, 1996; *Kukkonen and Peltonen*, 1999]. For this geotherm the lithosphere-asthenosphere boundary is assumed to be at 250 km depth. The overall velocity of the rock is calculated using the Voigt-Reuss-Hill average, which gives the same average values as the more accurate Hashin-Shtrikman averaging but is easier to compute [*Vacher et al.*, 1996]. Following *Goes et al.* [2000], we also take into account anharmonicity and an-

elasticity. Influence of the  $Q$  model on the composition-based velocities is low [Goes *et al.*, 2000; Bruneton *et al.*, 2004]. Different values for the elastic parameters and the  $Q$  model within a reasonable range can shift the obtained  $V_s(z)$  curves toward slightly lower or higher velocities, but all the models still have a negative gradient of shear wave velocity with depth.

[62] The family in Figure 11g in the southwestern part of the array is located in the Svecofennian domain. These profiles have velocities compatible with a normal composition from 100 km depth down to 150 km (depth of loss of resolution of our model). For the shallower mantle the velocities are lower in the surface wave derived profiles; however, it is the part of our model where the uncertainties are higher and these variations may not be significant. In particular, if we consider the 1% increase in absolute velocity produced by using the second initial model (see section 4.3.1), the surface wave derived velocities become compatible with the theoretical values below 70 km depth.

[63] In the northwestern region, Figure 11a presents normal velocities for the lower part of the model below 140 km and significantly lower velocities for the upper part of the lithospheric mantle. New interpretation of the geology of the Baltic Shield yields a complex history for the formation of the Svecofennian domain [Nironen *et al.*, 2002]. Nironen *et al.* present a map of the current position of lithospheric blocks that accreted around 2 Ga. The location of our Figure 11a family corresponds to the Knaften arc. The subduction that produced the volcanic arc is likely to have introduced a certain amount of water in the upper part of the mantle. Injection of water in the mantle is known to reduce the seismic velocities (see, e.g., results from the Tornquist-Teisseyre zone [Nolet and Zehuijs, 1994]).

[64] The family in Figure 11i has an anomalous velocity profile: almost constant for all depths. The southeastern corner of the SVEKALAPKO array where this family is located corresponds to the surface location of the Rapakivi granitoids. As these rocks are associated with mafic dikes derived from upper mantle partial melts [Korja *et al.*, 1993], they are thought to be of deep origin. Our model suggests that they are associated with an anomaly extending to at least 150 km.

[65] The Archean domain (Figure 11c) is the most difficult to interpret. The velocity seems compatible with normal peridotite immediately below the Moho to 90 km depth, a low-velocity zone is located at 140 km depth, followed by increasing velocities. A metasomatism of deep origin could have lowered the velocities from the bottom of the lithosphere without reaching the surface. The increasing velocities deeper than 140 km could be an artifact of our horizontal smoothing.

[66] The above interpretations are subject to change in the light of new geological interpretations or new geochemical analysis, but our results show the necessity of both vertical and lateral compositional variations in the Fennoscandian shield. The hypothesis of a high degree of heterogeneity in the lithosphere of the Svecofennian domain also correlates well with the observations of a complex pattern of crustal conductivity in Fennoscandia [Korja *et al.*, 2002]. The history of the Baltic Shield appears to be more complex than that of the Kaapvaal craton in South Africa [Fouch *et*

*al.*, 2004; James *et al.*, 2001], the Australian continent [Simons *et al.*, 2002; Debayle and Kennett, 2000], or the North American craton [van der Lee and Nolet, 1997] where the seismic tomography is closely related to surface features. In particular, these cratons generally exhibit higher velocities underneath Archean than Proterozoic terrains, which is the trend predicted from a larger depletion degree during the Archean [Jordan, 1979] and is not observed in the Baltic Shield.

## 6. Conclusions

[67] We conducted an inversion of fundamental mode Rayleigh wave travel time data to obtain a regional 3-D shear wave velocity model under a dense array of stations in the central Baltic Shield. The method used is based on two-dimensional ray tracing which is innovative in that the curvature of the wave fronts is taken into account.

[68] Our final shear wave velocity model shows lateral variations at each depth of  $\pm 3\%$  around the average value. Heat flow [Kukkonen, 1993] and receiver function analysis [Alinaghi *et al.*, 2003] require a very homogeneous thermal pattern for the upper mantle in the region. The lateral variations of seismic velocities are therefore most probably due to chemical variations.

[69] The obtained velocities are on average 4% higher than standard Earth models for the upper mantle down to 200 km. There is no evidence for a substantial low-velocity zone which would make it possible to define the lithosphere-asthenosphere boundary. Another criterion for defining this boundary would be the depth below which the amplitude of the lateral heterogeneities strongly diminishes, but our lateral resolution is poor below 150 km depth.

[70] The classification of the  $V_s(z)$  curves yields the definition of nine different regions that we interpret in terms of different rock composition and layering. Four main families can be reasonably associated to geological surface features: one is attributed to the Archean domain, and the three others can be correlated with the surface location of lithospheric blocks in the Proterozoic Svecofennian domain. Five intermediate families could be due to the smoothing introduced by the tomography, to slanting transitions, or to the presence of different compositions. However, this complex pattern is in agreement with other recent geophysical and geological studies in the area.

[71] Our results highlight the lateral and vertical compositional changes of the lithosphere within this shield area. However, even though there is a good correlation between the location of the families of shear wave velocities variations with depth and the main tectonic units, the results are significantly more complex than expected before the SVEKALAPKO seismic tomography experiment. This leads us to question the validity of simplistic compositional models of ancient lithosphere.

[72] **Acknowledgments.** We thank the numerous people who took part in the field work, as well as the numerous people who took part in it. The French participation received financial support from the Intérieur de la Terre program of INSU and used Lithoscope and RLBM seismic stations. We thank Valérie Maupin and Jean-Jacques Lévêque for the dispersion curve inversion code, and Ilmo Kukkonen for the regional geotherm and the xenolith-based seismic velocity model. This paper highly benefited from discussions with Michel Bouchon and from constructive reviews by Jeannot Trampert, an anonymous reviewer, and an anonymous associate editor. The

European Science Foundation financed most of the workshops of the SVEKALAPKO project. Most of the computations presented in this paper were performed at the Service Commun de Calcul Intensif de l'Observatoire de Grenoble (SCCI). We used SAC for the treatment of the seismograms. Figure 2 was drawn using GMT.

## References

- Aki, K., and P. G. Richards (2002), *Quantitative Seismology*, 2nd ed., 700 pp., Univ. Sci. Books, Sausalito, Calif.
- Alinaghi, A., G. Bock, R. Kind, W. Hanka, K. Wylegalla, TOR and SVEKALAPKO Groups (2003), Receiver function analysis of the crust and upper mantle from the North German Basin to the Archean Baltic Shield, *Geophys. J. Int.*, *155*, 641–652.
- Babuška, V., J. Plomerová, and P. Pajdušák (1988), Seismologically determined deep lithosphere structure in Fennoscandia, *Geol. Foeren. Stockholm Foerh.*, *110*, 380–382.
- Bock, G., and the SVEKALAPKO Seismic Tomography Working Group (SSTWG) (2001), Seismic probing of the Fennoscandian lithosphere, *Eos Trans. AGU*, *82*, 621, 628–629.
- Bruneton, M., V. Farra, H. A. Pedersen, and the SVEKALAPKO Seismic Tomography Working Group (2002), Non-linear surface wave phase velocity inversion based on ray theory, *Geophys. J. Int.*, *151*, 583–596.
- Bruneton, M., H. A. Pedersen, V. Farra, N. T. Arndt, P. Vacher, and the SVEKALAPKO Seismic Tomography Working Group (2004), Layered lithospheric mantle in the central Baltic Shield from surface waves and xenoliths analysis, *Earth Planet. Sci. Lett.*, in press.
- Calcagnile, G. (1982), The lithosphere-asthenosphere system in Fennoscandia, *Tectonophysics*, *90*, 19–35.
- Calcagnile, G. (1991), Deep structure of Fennoscandia from fundamental and higher mode dispersion of Rayleigh waves, *Tectonophysics*, *195*, 139–149.
- Cotte, N., H. A. Pedersen, M. Campillo, J. Ni, R. Kind, E. Sandvol, and W. Zhao (1999), Determination of the crustal structure in south Tibet by dispersion and amplitude analysis of surface waves, *Geophys. J. Int.*, *138*, 809–819.
- Debayle, E., and B. L. N. Kennett (2000), The Australian continental upper mantle: Structure and deformation inferred from surface waves, *J. Geophys. Res.*, *105*, 25,423–25,450.
- De Boor, C. (1978), *A Practical Guide to Splines*, 392 pp., Springer-Verlag, New York.
- Deschamps, G. A. (1972), Ray techniques in electromagnetics, *Proc. IEEE*, *60*, 1022–1035.
- Dziewonski, A. M., and D. L. Anderson (1981), Preliminary reference Earth model, *Phys. Earth Planet. Inter.*, *25*, 297–356.
- Farra, V., and R. Madariaga (1987), Seismic waveform modeling in heterogeneous media by ray perturbation theory, *J. Geophys. Res.*, *92*, 2697–2712.
- Fouch, M. J., D. E. James, J. C. Vandecar, S. van der Lee, and the Kaapvaal Seismic Group (2004), Mantle seismic structure beneath the Kaapvaal and Zimbabwe cratons, *S. Afr. J. Geol.*, *107*, 33–44.
- Friederich, W. (2003), The *S*-velocity structure of the east Asian mantle from inversion of shear and surface waveforms, *Geophys. J. Int.*, *153*, 88–102.
- Friederich, W., E. Wielandt, and S. Stange (1994), Non-plane geometries of seismic surface wavefields and their implications for regional surface-wave tomography, *Geophys. J. Int.*, *119*, 931–948.
- Gee, D. G., and H. J. Zeyen (Eds.) (1996), *EUROPROBE 1996—Lithosphere Dynamics: Origin and Evolution of Continents*, 138 pp., EUROPROBE Secretariat, Uppsala Univ., Uppsala, Sweden.
- Goes, S., R. Gover, and P. Vacher (2000), Shallow mantle temperatures under Europe from *P* and *S* wave tomography, *J. Geophys. Res.*, *105*, 11,153–11,169.
- Gorbatshev, R., and S. Bogdanova (1993), Frontiers in the Baltic Shield, *Precambrian Res.*, *64*, 3–21.
- Herrin, E., and T. Goforth (1977), Phase-matched filters: Application to the study of Rayleigh waves, *Bull. Seismol. Soc. Am.*, *67*, 1259–1275.
- Hjelt, S.-E., and J. S. Daly (1996), SVEKALAPKO, evolution of Paleoproterozoic and Archean lithosphere, in *EUROPROBE 1996—Lithosphere Dynamics: Origin and Evolution of Continents*, edited by D. G. Gee and H. J. Zeyen, pp. 57–67, EUROPROBE Secretariat, Uppsala Univ., Uppsala, Sweden.
- Husebye, E. S., and J. Hovland (1982), On upper mantle seismic heterogeneities beneath Fennoscandia, *Tectonophysics*, *90*, 1–17.
- Hwang, H. J., and B. J. Mitchell (1986), Interstation surface wave analysis by frequency-domain Wiener deconvolution and modal isolation, *Bull. Seismol. Soc. Am.*, *76*, 847–864.
- James, D. E., M. J. Fouch, J. C. Vandecar, S. van der Lee, and the Kaapvaal Seismic Group (2001), Tectospheric structure beneath southern Africa, *Geophys. Res. Lett.*, *28*, 2485–2488.
- Jordan, T. H. (1979), The deep structure of the continents, *Sci. Am.*, *240*, 92–107.
- Kennett, B. L. N., and K. Yoshizawa (2002), A reappraisal of regional surface wave tomography, *Geophys. J. Int.*, *150*, 37–44.
- Kennett, B. L. N., E. R. Engdhal, and R. Buland (1995), Constraints on seismic velocities in the Earth from traveltimes, *Geophys. J. Int.*, *122*, 108–124.
- Korja, A., T. Korja, U. Luosto, and P. Heikkinen (1993), Seismic and geoelectric evidence for collisional and extensional events in the Fennoscandian Shield—Implication for Precambrian crustal evolution, *Tectonophysics*, *219*, 129–152.
- Korja, T., et al. (2002), Crustal conductivity in Fennoscandia—A compilation of a database on crustal conductance in the Fennoscandian Shield, *Earth Planets Space*, *54*, 535–558.
- Kozlovskaya, E., S. E. Hjelte, J. Yliniemi, M. Pirttijärvi, and The SVEKALAPKO Seismic Tomography Working Group (2004), 3D density model of the crust of southern and central Finland obtained from joint interpretation of SVEKALAPKO crustal *P*-wave velocity model and gravity data, *Geophys. J. Int.*, doi:10.1111/j.1365-246X.2004.02363.x.
- Kukkonen, I. T. (1993), Heat-flow map of northern and central parts of the Fennoscandian Shield based on geochemical surveys of heat producing elements, *Tectonophysics*, *225*, 3–13.
- Kukkonen, I. T., and A. Jöeleht (1996), Geothermal modelling of the lithosphere in the central Baltic Shield and its southern slope, *Tectonophysics*, *255*, 24–45.
- Kukkonen, I. T., and P. Peltonen (1999), Xenolith-controlled geotherm for the central Fennoscandian Shield: Implications for lithospheric-asthenospheric relations, *Tectonophysics*, *304*, 301–315.
- Kukkonen, I. T., K. Kinnunen, and P. Peltonen (2003), Mantle xenoliths and thick lithosphere in the Fennoscandian Shield, *Phys. Chem. Earth*, *28*, 349–360.
- Lander, A. V., and A. L. Levshin (1989), Recording, identification, and measurement of surface wave parameters, in *Seismic Surface Waves in Laterally Inhomogeneous Earth*, edited by V. I. Keilis-Borok, pp. 131–182, Kluwer Acad., Norwell, Mass.
- Lévêque, J.-J., M. Cara, and D. Rouland (1991), Waveform inversion of surface wave data: Test of a new tool for systematic investigation of upper mantle structures, *Geophys. J. Int.*, *104*, 565–581.
- Maupin, V., and M. Cara (1992), Love-Rayleigh wave incompatibility and possible deep upper mantle anisotropy in the Iberian peninsula, *Pure Appl. Geophys.*, *138*, 429–444.
- Nataf, H.-C., and Y. Ricard (1996), 3SMAC: An a priori tomographic model of the upper mantle based on geophysical modeling, *Phys. Earth Planet. Inter.*, *95*, 101–122.
- Nironen, M., R. Lahtinen, and A. Korja (2002), Paleoproterozoic tectonic evolution of the Fennoscandian shield—Comparison to modern analogues, in *Lithosphere 2002—Second Symposium on the Structure, Composition and Evolution of the Lithosphere in Finland, Programme and Extended Abstracts, Espoo, Finland*, edited by R. Lahtinen et al., *Rep. S-42*, pp. 95–97, Inst. of Seismol., Univ. of Helsinki, Helsinki, Finland.
- Nolet, G., and F. A. Dahlen (2000), Wave front healing and the evolution of seismic delay times, *J. Geophys. Res.*, *105*, 19,043–19,054.
- Nolet, G., and A. Zehuis (1994), Low *S* velocities under the Tornquist-Tesseyre zone: Evidence for water injection into the transition zone by subduction, *J. Geophys. Res.*, *99*, 15,813–15,820.
- Pearson, D. G., G. J. Irvine, R. W. Carlson, M. G. Kopylova, and D. A. Ionov (2002), The development of lithospheric keels beneath the earliest continents: time constraints using PGE and Re-Os isotope systematics, in *The Early Earth: Physical, Chemical and Biological Development*, edited by C. M. R. Fowler, C. J. Ebinger, and C. J. Hawkesworth, *Geol. Soc. Spec. Publ.*, *199*, 65–90.
- Plomerová, J., T. Hyvönen, V. Babuška, L. Vecsey, T. Raita, the SVEKALAPKO Seismic Tomography Working Group, and the TOR Working Group (2003), Seismic-wave anisotropy of the subcrustal lithosphere of Fennoscandia based on body-wave data recorded during the international passive experiments, paper presented at EGS-AGU-EUG Joint Meeting, Nice, France.
- Röhm, A. H., R. K. Snieder, S. Goes, and J. Trampert (2000), Thermal structure of the continental upper mantle inferred from *S* wave velocity and surface heat flow, *Earth Planet. Sci. Lett.*, *181*, 395–408.
- Sacks, I. S., J. A. Snoke, and E. S. Husebye (1979), Lithosphere thickness beneath the Baltic Shield, *Tectonophysics*, *56*, 101–110.
- Saito, M. (1988), Disper 80: A subroutine package for the calculation of seismic modes solutions, in *Seismological Algorithms*, edited by D. J. Doornbos, pp. 293–319, Academic, San Diego, Calif.
- Sandoval, S., E. Kissling, J. Ansorge, and the SVEKALAPKO Seismic Tomography Working Group (2003), High-resolution body wave tomography beneath the SVEKALAPKO array: I. A priori 3D crustal model and associated traveltime effects on teleseismic wavefronts, *Geophys. J. Int.*, *153*, 75–87.

- Sandoval, S., E. Kissling, J. Ansorge, and the SVEKALAPKO Seismic Tomography Working Group (2004), High-resolution body wave tomography beneath the SVEKALAPKO array: II. Anomalous upper mantle structure beneath central Baltic Shield, *Geophys. J. Int.*, *157*, 200–214.
- Simons, F. J., R. D. van der Hilst, J.-P. Montagner, and A. Zielhuis (2002), Multimode Rayleigh wave inversion for heterogeneity and azimuthal anisotropy of the Australian upper mantle, *Geophys. J. Int.*, *151*, 738–754.
- Spetzler, J., J. Trampert, and R. Snieder (2002), The effect of scattering in surface wave tomography, *Geophys. J. Int.*, *149*, 755–767.
- Tarantola, A. (1987), *Inverse Problem Theory: Methods for Data Fitting and Parameter Estimation*, 613 pp., Elsevier Sci., New York.
- Tarantola, A., and B. Valette (1982), Generalized nonlinear inverse problems solved using the least square criterion, *Rev. Geophys.*, *20*, 219–232.
- Tryggvason, E. (1961), Crustal thickness in Fennoscandia from phase velocities of Rayleigh waves, *Ann. Geofis.*, *14*, 267–293.
- Vacher, P., A. Mocquet, and C. Sotin (1996), Comparison between tomographic structures and models of convection in the upper mantle, *Geophys. J. Int.*, *124*, 45–56.
- van der Lee, S., and G. Nolet (1997), Upper mantle *S* velocity structure of North America, *J. Geophys. Res.*, *102*, 22,815–22,838.
- Wielandt, E. (1993), Propagation and structural interpretation of non-plane waves, *Geophys. J. Int.*, *113*, 45–53.
- Wiener, N. (1949), *Time Series*, 163 pp., M.I.T. Press, Cambridge, Mass.
- U. Achauer, Ecole et Observatoire des Sciences de la Terre, University of Strasbourg, 5 Rue Rene Descartes, F-67084 Strasbourg, France.
- A. Alinaghi and K. Wilegalla, GeoForschungsZentrum Potsdam, Telegrafenberg Haus E, D-14473 Potsdam, Germany.
- J. Ansorge, E. Kissling, and S. Sandoval, Institute of Geophysics, ETH Zurich, CH-8093 Zurich, Switzerland.
- N. T. Arndt, Laboratoire de Géodynamique des Chaînes Alpines, Université Joseph Fourier, BP 53, F-38041 Grenoble cedex 9, France.
- M. Bruneton and H. A. Pedersen, Laboratoire de Géophysique Interne et Tectonophysique, Université Joseph Fourier, BP 53, F-38041 Grenoble cedex 9, France. (marianne.bruneton@obs.ujf-grenoble.fr; pedersen@obs.ujf-grenoble.fr)
- V. Farra, Département de sismologie, Institut de Physique du Globe de Paris, 4 Place Jussieu, F-75252 Paris Cedex 5, France. (farra@ipgp.jussieu.fr)
- W. Friederich and E. Wielandt, Institute of Geophysics, University of Stuttgart, Richard-Wagner-Str. 44, D-70184 Stuttgart, Germany.
- M. Grad, Institute of Geophysics, University of Warsaw, Pasteura 7, Warsaw, 02-093, Poland.
- A. Guterch, Institute of Geophysics, Department of Seismology, Polish Academy of Sciences, Ks. Janusza 64, Warsaw, 01-452, Poland.
- P. Heikkinen, T. L. Hyvönen, J.-P. Ikonen, and A. Korja, Institute of Seismology, University of Helsinki, P.O. Box 26, 00014 Helsinki, Finland.
- S.-E. Hjelt, K. Komminaho, E. Kozlovskaya, T. Raita, and J. Tiikkainen, Department of Geophysics, University of Oulu, Oulu, FIN-90014 Finland.
- M. V. Nevsky, N. I. Pavlenkova, O. Y. Riznichenko, and I. A. Sanina, Institute of Physics of the Earth, Russian Academy of Sciences, Moscow, Russia.
- H. Paulssen, Utrecht University, P.O. Box 80.021, NL-3508 TA Utrecht, Netherlands.
- J. Plomerová, Geophysical Institute of Academy of Sciences of the Czech Republic, 14131 Prague, Czech Republic.
- R. G. Roberts and Z. H. Shomali, Department of Earth Sciences, University of Uppsala, Villavägen 16, SE-75236 Uppsala, Sweden.
- N. V. Sharov, Kola Scientific Center, Russian Academy of Sciences, Apatity, Russia.
- P. Vacher, Laboratoire de Planétologie et Géodynamique, Faculté des Sciences et techniques, 2 rue de la Houssinière, F-44322 Nantes Cedex 3, France. (vacher@chimie.univ-nantes.fr)
- J. Yliniemi, Sodankylä Geophysical Observatory Oulu Unit, University of Oulu, FIN-90014 Oulu, Finland.
- Y. G. Yurov, Spezgeofisika MNR, Nizhnaja Krasnoselskaya 4, Moscow 107140, Russia.